

Received March 16, 2021, accepted March 21, 2021, date of publication March 29, 2021, date of current version April 9, 2021.

Digital Object Identifier 10.1109/ACCESS.2021.3069549

# Force Perception and Bone Recognition of Vertebral Lamina Milling by Robot-Assisted Ultrasonic Bone Scalpel Based on Backpropagation Neural Network

HAO QU<sup>1</sup>, BAODUO GENG<sup>2</sup>, BINGRONG CHEN<sup>1</sup>, JIAN ZHANG<sup>2</sup>,  
YONGLIANG YANG<sup>1,3</sup>, (Member, IEEE), LEI HU<sup>2</sup>, AND YU ZHAO<sup>1</sup>

<sup>1</sup>Department of Orthopedics, Peking Union Medical College Hospital, Chinese Academy of Medical Sciences and Peking Union Medical College, Beijing 100730, China

<sup>2</sup>School of Mechanical Engineering and Automation, Beihang University, Beijing 100191, China

<sup>3</sup>State Key Laboratory of Internet of Things for Smart City, Faculty of Science and Technology, University of Macau, Macau 999078, China

Corresponding authors: Yu Zhao (zhaoyupumch@126.com) and Lei Hu (hulei9971@sina.com)

This work was supported in part by the National Key Research and Development Program of China under Grant 2018YFB1307603, and in part by the Beijing Natural Science Foundation under Grant L182068.


**ABSTRACT** With the development of artificial intelligence technologies, spine-surgery robots have gradually been applied in clinical practice, and they have exhibited favorable development prospects. Force perception technology can be used to obtain the milling force, quantify the tactile sensation of a surgeon, and provide feedback or suggestions to the surgeon and robot for safe milling. In this study, a robotic system is proposed to measure the vertebral lamina milling force by using an ultrasonic bone scalpel to realize a safe milling strategy. The developed bone recognition model based on the backpropagation neural network is suitable for robot-assisted vertebral lamina milling using the milling delamination and recognition algorithm analysis. The model uses the characteristic milling force, milling speed, milling depth, and ultrasonic scalpel power as inputs to determine whether milling has reached the inner cortical bone to recognize and judge bone layers. The verification experiment on live animals showed that this model could accurately determine a safe milling endpoint. In general, this recognition model can significantly improve the safety and reliability of robot-assisted laminectomy and has significant translational prospects.

**INDEX TERMS** Bone recognition, force perception, neural network, robot, ultrasonic scalpel, vertebral lamina.

## I. INTRODUCTION

In recent years, there has been an increase in the incidence of spinal diseases represented by lumbar spinal stenosis and lumbar disc herniation. At present, surgery is the most effective treatment to remove spinal lesions and relieve the related symptoms that seriously affect a patient's quality of life [1]–[3]. Generally, spinal decompression surgery is performed by partially or completely removing the vertebral lamina to relieve compression on the spinal cord caused by spinal stenosis, combined with a pedicle screw fixation system to maintain spine stability. However, the surgeon must

perform complex and delicate surgeries in a small surgical field. In addition, the surgery can be significantly difficult and risky, with severe complications and extremely high dependency on the surgeon. For improving surgery safety, artificial intelligence technologies, such as spine-surgery robots with high accuracies and degrees of freedom, have shown favorable development prospects and gradually been applied in clinical practice [4]–[6]. Studies have shown that the system error of the Mazor Robotics Renaissance guidance system is less than 1 mm, and the operation accuracy rate can reach 98.3% [7]. Because there are important spinal cords, nerve roots, and blood vessels around the vertebral lamina, serious injury and even paralysis can easily occur if the milling scope exceeds the edge of the vertebral lamina during operation [8].

The associate editor coordinating the review of this manuscript and approving it for publication was Chua Chin Heng Matthew .

Therefore, it is essential to obtain more information on the operation status during robot-assisted surgery and recognize the tissue in contact with the robotic arm end.

In traditional manual surgery, surgeons mainly use their tactile sensations to judge the nature of the milled tissue. The force feedback from the surgical instrument combined with the surgeon's experience is used to determine the type of the contacted bone layer. Therefore, some surgical-robot studies have simulated this judgment process using force perception technology to determine the milling force, quantify the surgeon's sensation, and provide feedback or suggestions to the surgeon for safe robotic milling [9], [10]. The tactile sensation of the surgeons corresponds to the force control of the surgical robot. In the field of robotics, researchers have developed various high-performance force controllers [11]. One of the most representative controllers is the "impedance control" proposed by Hogan [12], and it establishes the dynamic relationship between the position and force of the manipulator end-effector. "Admittance control" and various "hybrid controllers" have been proposed and widely used in robotics research [13]. Although the application of high-performance force controllers in robot-assisted spinal surgery will be the future, it is necessary to design specific force controllers for different bone tissues because of the complex bone structure of the vertebral lamina. Therefore, the accurate use of force perception for bone recognition is the premise of force controller research [14].

Based on the milling force perception, Marco *et al.* constructed a milling force model for an electric drill using finite element analysis and concluded that the milling force is positively correlated with bone density for bone tissue recognition [15]. Hu *et al.* designed a real-time force sensor algorithm for measurements during operation and initially judged the bone layer based on the milling force [16]. In some studies, the feasibility and effectiveness of bone recognition models have been verified based on force perception using artificial intelligence algorithms. Fan *et al.* used the milling force in the horizontal direction as a controlled constant with fuzzy force control logic and milling force in the vertical direction to distinguish the bone layer structure [17]. Kasahara *et al.* developed a system that determines both the motion and cutting states from demonstrations using support vector machines (SVMs) based on the motor current, rotational speed of the cutting tool, and output of an acceleration sensor [18]. Kais *et al.* developed artificial neural network models of bone milling force based on an experimental study using cancellous bone and validated the models for the specified bone type, milling parameter range, and milling tool type [19]. Some studies have also established milling state recognition and control methods by collecting force data in real time and calculating the energy attenuation after milling different bones, to realize the parking control of the milling endpoint [20]. In other studies, the vibration amplitude at the end of the drill, frequency and loudness of the milling sound, temperature of the milling parts, and current change of the drill were obtained and monitored to indirectly reflect

the mechanical information during bone milling and realize bone tissue recognition [20]–[23]. However, these studies did not consider the different operative methods, speed, and parameter settings of the power equipment, which eventually affect the perception of the milling force. In addition, these models were not experimentally verified by using them in a real surgical environment or on animals.

The aforementioned studies confirmed that the milling force can reflect the mechanical properties of the local bone layer in real time and can be used as an important basis for bone recognition. However, at present, electric drills are typically used as milling tools in robot-assisted laminectomy, and in most of the related force-perception studies, the end force data were collected for modeling. Although electric drills can quickly mill bone tissue, they have shortcomings such as large mechanical vibrations, high heat production, unstable control, and proneness to damaging surrounding soft tissue. This not only affects the stability of the force signal and increases the difficulty in bone recognition but also increases the surgical risk. In recent years, novel ultrasonic bone scalpels have gradually been adopted in orthopedic surgery. The principle of the ultrasonic bone scalpel, which was first developed by Tomaso in 1988, is the use of high-intensity focused ultrasound to convert electrical energy into mechanical energy and cut tissue by utilizing high-frequency ultrasonic vibrations [24]. The working frequency of ultrasonic bone scalpels is generally 25–30 kHz, which can cause direct mechanical damage to bone tissue with a high acoustic impedance, and the energy range is only a few hundred millimeters. This cannot cut soft tissues such as muscles, blood vessels, or mucous membranes and, therefore, has the advantages of accurate bone cutting and prevention of soft tissue scraping; combined with a pressure sensor, this can achieve a strong hard-tissue-recognition function [25]–[27]. The swing amplitude of the ultrasonic blade is 60–200  $\mu\text{m}$  in the horizontal direction and 20–60  $\mu\text{m}$  in the vertical direction with small and regular vibrations, and the contact area with the bone tissue is uniform. Compared with electric drills, the milling force signal from ultrasonic scalpels is smoother, bone surface after milling is smoother and flatter, and fewer interference factors exist [28], [29]. However, research on milling force perception based on ultrasonic power has not been reported yet.

The purpose of this study is to explore the force perception and bone recognition of ultrasonic bone scalpels for robot-assisted vertebral lamina milling based on a back-propagation (BP) neural network to achieve a safe milling strategy. First, the force signals in vertebral lamina milling are collected by using a six-axis force sensor and processed by an applicable wavelet transform denoising method. Then, a BP neural network is established, which takes the force information and milling influencing factors as the input and outputs bone information to realize bone layer recognition and safe milling. Finally, a live animal experiment is performed to verify the feasibility and accuracy of the proposed model.

The rest of the article is structured as follows. Section II describes the vertebral lamina milling operation with the ultrasonic scalpel. Section III introduces the strategy and hardware platform composition of robot-assisted vertebral lamina milling. Section IV presents a recognition algorithm for the milling system based on force perception. Section V describes the verification experiments on live animals. Finally, the conclusions are given in Section VI.

## II. VERTEBRAL LAMINA MILLING BY ULTRASONIC SCALPEL

The bone structure of the vertebral lamina is composed of the outer and inner cortical bone and inner cancellous bone in a sandwich-like structure. The cortical bone, which has a high density, high strength, and smooth surface, acts as a supporting structure and protects the spinal cord. The spongy, low-density cancellous bone serves to improve the structural filling and impact resistance [30], [31]. The density, strength, and mechanical properties of each bone layers are different. During the vertebral lamina milling operation, the end-effector of the manipulator mills the outer cortical bone, cortical–cancellous bone junction, cancellous bone, cancellous–cortical bone junction, and inner cortical bone of the vertebral lamina in a layer-by-layer fashion [32]. A study by Van Ham *et al.* found that the average milling force generated using a drill for bone milling was exponentially related to the bone density measured by quantitative computed tomography [33]. They also showed that under normal conditions, the force generated by the device when milling cortical bone is greater than that during milling bone junctions or cancellous bone. Therefore, we used the strong correlation between the bone structure of the vertebral lamina and milling force to analyze the changes in milling force throughout the operation by collecting real-time force data as the robot milled the vertebral lamina, thereby realizing real-time recognition of the milled bone layer.

In terms of milling tool selection, the ultrasonic bone scalpel has advantages such as precise milling, stability, and safety. In addition, the improved force signal characteristics and enhanced bone tissue recognition make it highly suitable for force perception research in the field of robotics. Therefore, based on clinical needs and engineering requirements, an ultrasonic bone scalpel (Beijing Sonicmed Technology) was selected as the milling tool in the proposed robot-assisted vertebral lamina milling system [34]. The ultrasonic scalpel was equipped with a special bone milling handle and milling drill, which meets the requirements of the proposed milling strategy.

In this study, a surgeon and engineer decided the scope of vertebral lamina milling by jointly operating the robot. The start and end points of the milling path were typically located medial to the articular processes of the spine. The milling length was approximately 15–20 mm, depth was approximately 8–10 mm, and width was 3.5 mm. The robot was equipped with an ultrasonic scalpel bone milling handle, which automatically performed layer-by-layer milling

within the specified ranges. The single-layer milling operation was divided into three processes: sinking, feeding, and back milling. In the sinking process, the ultrasonic scalpel mills down the specified distance along the normal direction of the vertebral lamina tangent plane at the starting point to reach the single-layer milling depth. During the feeding process, the drill mills at a constant speed in the horizontal direction from the starting to the ending position to complete the single-layer milling. In the back-milling process, the drill mills back from the end to the start positions at a constant speed in the horizontal direction to clean up bone and residue that were not milled at the edge of the milling track during the feeding process to ensure that the milling force signal in the next layer is not affected by the previous layer (Fig. 1).

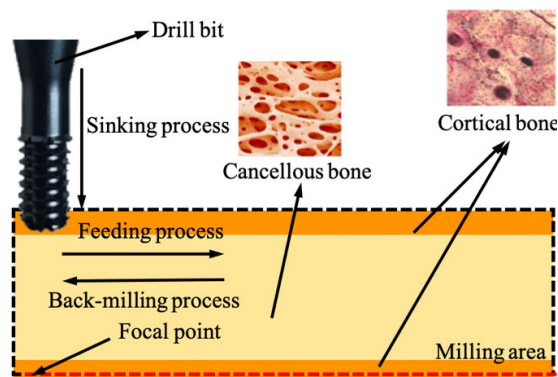


FIGURE 1. Operation of single-layer vertebral lamina milling.

## III. HARDWARE PLATFORM FOR VERTEBRAL LAMINA MILLING FORCE

### A. VERTEBRAL LAMINA MILLING STRATEGY

The robot milling system in this study adopted the following safe milling strategy (Fig. 2). Throughout the milling process, the implemented robot controller acted as the position servo control system inside the robot, with a control frequency of 100 Hz. The robotic system used a force sensor to collect the force signal at the robotic arm end in real time and filter the force signal of each layer. The calculated average value was then input into the BP neural network to recognize each bone layer. The thickness of the inner cortical bone of the vertebral lamina is approximately 1–2 mm. Therefore, the system automatically stops when the milling depth reaches a thickness of 1 mm in the inner cortical bone to ensure that the vertebral lamina could be removed without being completely milled. Thus, safe milling is achieved by ensuring that the spinal cord and nerve roots are not damaged.

### B. SYSTEM HARDWARE PLATFORM

The robotic system for vertebral lamina milling was built to achieve robot-assisted laminectomy and milling force perception. This system hardware platform includes a six-degree-of-freedom robotic arm with a trolley, a six-axis force sensor with a capture card, and an ultrasonic bone scalpel with a clamping end (Fig. 3). The theoretical analysis of the control

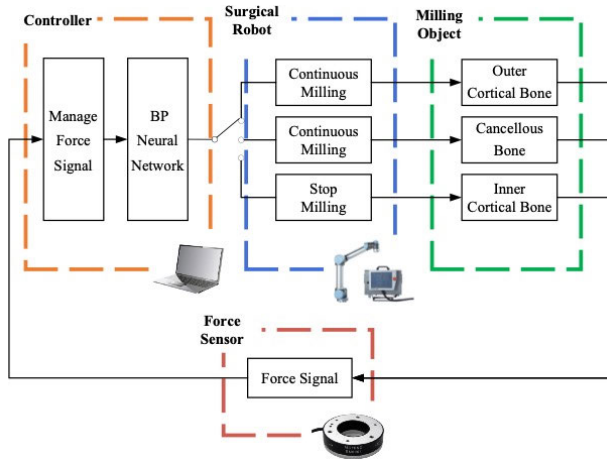


FIGURE 2. Safe milling strategy of the robot-assisted vertebral lamina milling system.

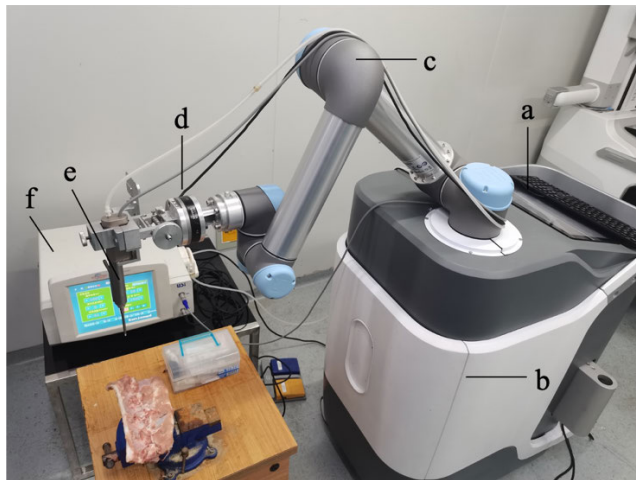


FIGURE 3. Operating platform of the robotic milling system: a) control computer; b) trolley; c) six-degree-of-freedom robotic arm; d) six-axis force sensor; e) ultrasonic scalpel milling tool handle and scalpel drill bit; f) ultrasonic scalpel host.

performance, such as position and force tracking accuracy, can be justified by using the Lyapunov stability principle [35], LaSalle invariance principle [36] and Barbalat’s lemma [37], which are not described in detail in this paper.

The robotic arm realized the bearing and positioning of the actuator to ensure sufficient working space during milling to stably and reliably accomplish the instructed movements. In this study, we used the collaborative Danish Universal Robots 5 (UR5). The UR5 robotic arm parameters (Table 1) meet the needs of the vertebral lamina milling tasks, with protection functions such as collision detection and emergency stopping to maximize patient safety [38].

The main task in this study was the collection and analysis of milling force signals. Therefore, the selection of the force sensor was particularly important. An M8128 force sensor (US SRI) and supporting digital acquisition card were selected for the system. This model uses a six-axis force sensor to simultaneously measure three forces and three

TABLE 1. UR5 parameters.

Parameter	Value	Dimension
Weight	18.4	kg
Radius	850	mm
Payload	5	kg
Joint range of motion	$\pm 180$	deg
Maximum speed	3	mm/s
Repeated positioning accuracy	$\pm 0.1$	mm

moments in the inertial coordinate system and collect milling force signals from various angles. The force sensor consists of an inner ring, outer ring, force measuring beam, and strain gauge. When there is a relative force between the inner and outer rings, the strain gauge detects the generated external force using the force measuring beam, converts it into an electrical signal, and outputs it to the acquisition card. The force measurement accuracy was within 2% FS. The digital acquisition card used a 24-bit sigma-delta analog-to-digital converter with a sampling frequency of up to 2 kHz to discretize the analog output of the force sensor, which was then sent to the host computer for processing through the RS232 protocol.

In addition, to facilitate the surgical disinfection process, the system employed the designed robotic arm end capable of fast clamping. The arm end could be rigidly connected to the six-axis force sensor and ultrasonic bone scalpel and was easy to disassemble, for convenient rapid end replacement during the operation. With different ends, a variety of surgical operations can be performed, and the ultrasonic scalpel can be clamped to the robotic arm end within 5 s after disinfection.

#### IV. MILLING FORCE PERCEPTION AND BONE RECOGNITION ALGORITHM

##### A. ANALYSIS OF VERTEBRAL LAMINA MILLING FORCE

The force signal from the ultrasonic bone scalpel while milling the vertebral lamina was transmitted to the host computer through the six-axis force sensor and acquisition card. Because the sampling frequency of the acquisition card was 2 kHz, and the force signal data were in the range of only 0–100 Hz, the original force signal transmitted by the acquisition card might contain high-frequency noise that could severely affect the accuracy of the subsequently applied neural network. Therefore, filtration of the raw force signal was essential. The force signal in the time domain was sometimes not intuitive. To perform noise reduction with frequency division, the frequency domain characteristics of the signal must first be understood. The Fourier transform is the most common process used to transform a signal from the time domain into the frequency domain [39]. For example, as shown in (1), Fourier transform can be used to analyze the sine wave component of the signal, which is convenient for judging the energy characteristics of the signal frequency band. Therefore, we first performed a fast Fourier transform on the raw force signal to obtain the corresponding frequency spectrum (Fig. 4).

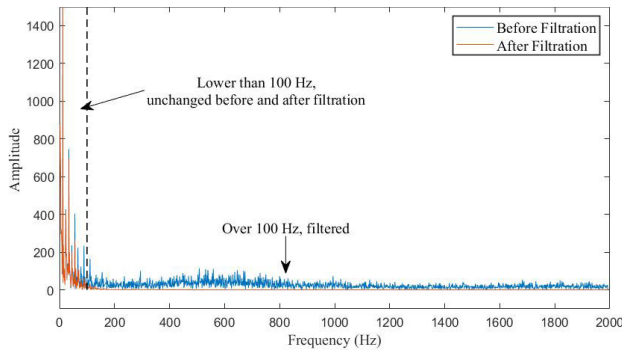


**FIGURE 4.** Spectrogram of ultrasonic scalpel milling force signal, where blue and orange lines represent the waveforms before and after filtering, respectively.

The blue waveform in the figure is the spectrogram of the original signal, which contains a significant amount of noise in the range of 100–2000 Hz. This noise should be selectively filtered out without affecting the force signal in the 0–100 Hz range.

$$F(\omega) = F[f(t)] = \int_{-\infty}^{\infty} f(t)e^{-i\omega t} dt \quad (1)$$

Although a Fourier transform can extract the frequency domain information of a signal, the local characteristic information cannot correspond to the time domain. Wavelet transform can effectively extract useless noise frequency bands for processing, has little impact on the time domain characteristics of the effective signal, and protects the signal peaks and transient signals. Therefore, we used noise reduction based on wavelet transform threshold processing to reduce the noise of the original force signal [40].

For discrete signals, DWT discrete wavelet transform processing, which is given by (2), is required.

$$\psi_{j,k}(t) = 2^{-j/2} \psi(2^{-j}t - k) \quad j, k \in Z, \quad (2)$$

where  $\psi(t)$  is the wavelet function,  $\psi_{j,k}(t)$  is the discrete wavelet function group, and  $j$  and  $k$  are the localization function parameters of the wavelet transform in the frequency and time domains, respectively.

Similar to the sine basis function of the Fourier transform, the wavelet transform also requires the definition of a basis function to decompose the signal. The output of the decomposed signal has two parts: a low-frequency component called the approximate component, which must be retained, and a high-frequency component called the detail component, which is filtered out. According to the Nyquist sampling theorem, the sampling frequency should be at least two times the signal frequency. Thus, multilayer wavelet decomposition is required for the original signal to select the effective frequency band by filtering. Then, the threshold is selected, and a soft threshold function is used to filter the high-frequency components. A soft threshold was chosen because denoising a hard threshold function will cause local jitter in the signal, whereas denoising a soft threshold function will make the

signal smoother [41]. Finally, the wavelet after threshold processing is reconstructed to obtain the pure force signal after filtering.

Based on the aforementioned theory, we established an applicable wavelet transform denoising method according to the characteristics of the force signal from ultrasonic scalpel milling of the vertebral lamina. The basis function of the system wavelet transform is a Daubechies series of wavelets, referred to as the dbN wavelet system, because of its good regularity—the signal reconstruction process is smooth [42]. These wavelet functions usually have no analytical expressions and are generally represented by filter banks. In this study, db4 was selected as the wavelet function.

The selection of the threshold after wavelet decomposition is based on (3).

$$X_n = f_n + e_n, \quad (3)$$

where  $X_n$  is the mixed signal with a length of  $N$ , and  $f_n$  and  $e_n$  are the data signal and white Gaussian noise signal  $N(0,1)$ , respectively, required for using the mixed signal to evaluate the threshold of eliminable noise in the wavelet domain. There are many common threshold methods, such as fixed threshold, extreme threshold, unbiased likelihood, and heuristic estimation methods. In this study, the Stein unbiased risk threshold, which are described by (4)–(6), was selected [36]. The absolute value of each element in signal  $X_n$  was removed and sorted in the decreasing order, and then the square of each element was acquired to obtain a new element sequence.

$$s(k) = (\text{sort}(|X|))^2. \quad (4)$$

If the square root of the  $k$ -th element with threshold  $s(k)$  is considered, the risk generated by the threshold is as follows.

$$\text{Risk}(k) = [N - 2k + \sum_{i=1}^k s(i) + (N - k)s(N - k)]/N. \quad (5)$$

According to the obtained risk curve  $\text{Risk}(k)$ , the value corresponding to the minimum risk point is recorded as  $k_{\min}$ . Then, the rigrsure threshold is defined as

$$\lambda_k = \sqrt{s(k_{\min})}. \quad (6)$$

After determining the threshold of white Gaussian noise in the wavelet domain, it is necessary to use a soft threshold function to filter the detailed components after wavelet decomposition. Once the parameters of each part are determined according to the above steps, the frequency domain characteristics of the signal are continuously adjusted according to the number of wavelet decomposition layers. The noise in the frequency band outside the 0–100 Hz range was found to be effectively filtered out when the number of wavelet decomposition layers was 5.

Taking the example of a set of force signals in the  $x$ -direction (vertical),  $y$ -direction (horizontal), and  $z$ -direction (vertical feed) from the milling process, we can obtain the time domain diagrams of the signal before and after wavelet

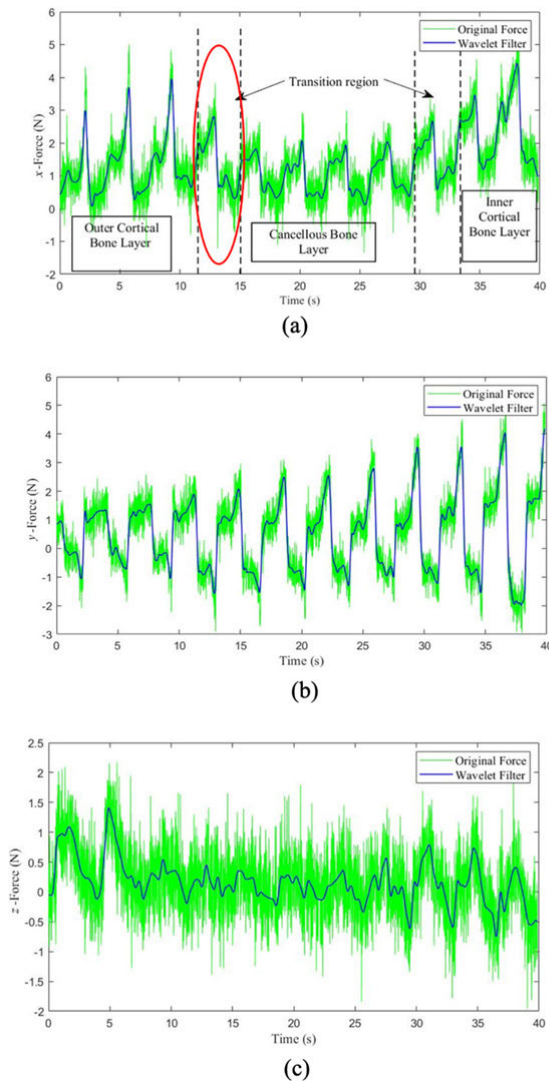


**FIGURE 5.** Original force signal in each direction and the signal after wavelet transform filtering: (a) x-direction (vertical), (b) y-direction (horizontal), and (c) z-direction (vertical feed), where the green and blue lines represent the waveforms before and after filtering, respectively.

transform filtering (Fig. 5), where the green and blue waveforms are the original and filtered force data, respectively. A comparison of these waveforms shows that the signal characteristics are completely retained after filtering, whereas the noise from the raw signal is filtered out.

Based on a combination of the bone structure, material properties, and imaging data of vertebral lamina from several tests [28]–[30], the most obvious correspondence was found to exist between the mechanical characteristics and lamina bone layer in the x-direction. Therefore, according to the milling strategy, different bone tissues could be recognized by comparing the mean values of force data of each layer in the x-direction during milling. The characterized results were as follows.

- 1) At 0–11 s, the milling force is relatively large (3–6 N). According to the structure and milling process of the

vertebral lamina, the milling area during this period can be inferred to be the outer cortical bone.

- 2) At 11–15 and 29.5–33 s, the milling force is intermediate (approximately 3 N), indicating that the drill bit is at the junction between the outer cortical bone and cancellous bone. Therefore, the signal corresponds to a transitional force.
- 3) At 15–29.5 s, the milling force is relatively small (0–3 N), indicating that the area milled during this time is the cancellous bone.
- 4) At 33–40 s, the milling force is again large (3–6 N), indicating that the area milled at this time is the inner cortical bone.

According to the established milling strategy, the depth of milling for each layer is 0.5 mm, and therefore milling is stopped after the inner cortical bone is milled by a maximum of two layers. To support this judgment, we carried out a milling experiment on an isolated spinal bone. The gross findings and CT images confirmed that this strategy could leave a thin layer in the inner cortical bone of the vertebral lamina, which meets the requirements of vertebral lamina milling (Fig. 6).

The time-domain diagram of the force in the y-direction of the ultrasonic bone scalpel during vertebral lamina milling shows that the force in this direction is affected by the milling depth. The peak overall force increases layer by layer, whereas there is no clear difference among different bones. In contrast, the time domain diagram of force in the z-direction has no obvious characteristics and cannot be used for bone recognition because of small contributions from lateral vibrations and milling with an ultrasonic bone scalpel.

We enlarged the single-layer milling force signal (red circle) in the x-direction in Fig. 7 to distinguish the whole sinking–feeding–back milling process:

- 1) The wave crest at 0–1.1 s represents the milling force during sinking; 2) the highest wave crest at 1.1–2.45 s represents the feeding milling force; 3) the lowest valley at 2.45–3.6 s represents the force of the back milling process. To differentiate between the milling forces of different bones more accurately, in this study, the milling force in the x-direction during the feeding process was selected as the characteristic force for neural network input. From the above analyses, judging the bone layer in the vertebral lamina milling process based on the force characteristics is feasible and only requires verification of the universality of this law and transformation into a mathematical model for use in actual milling operations.

## B. BONE RECOGNITION ALGORITHM BASED ON BP NEURAL NETWORK

Because the changes in milling force corresponding to different bone tissues belong to a regular model, they are difficult to explicitly define with general mathematical formulas. A large amount of experimental data must be used for training and verification to obtain a suitable model. Among the various

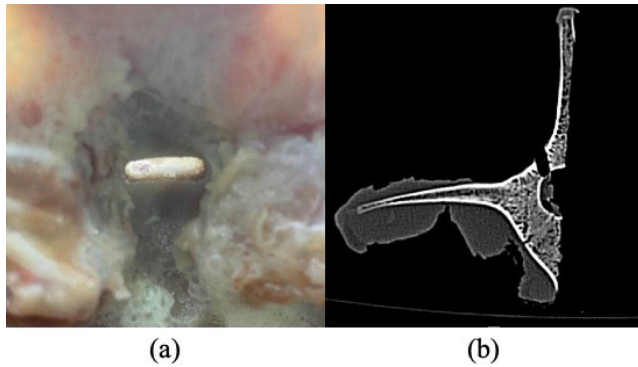


**FIGURE 6.** Experimental results of isolated bone vertebral lamina milling: (a) the photo of vertebral lamina after milling; (b) the CT image of the vertebral body.

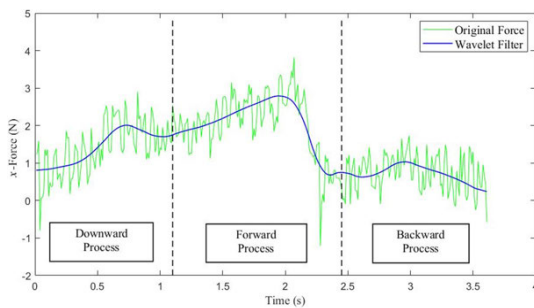


**FIGURE 7.** Original force signal and wavelet-filtered signal from the single-layer milling process, where green and blue lines represent the waveforms before and after filtering, respectively.

algorithmic models, a neural network is the most suitable model for this study.

In the process of vertebral lamina milling with an ultrasonic bone scalpel, a large amount of milling force data can be collected from the single-layer milling operation. In addition, these force signals have many influencing factors, such as milling speed, milling depth, and ultrasonic scalpel power. If all the force data and influencing factors are input into the neural network for training, it will greatly increase the calculation cost and bone recognition difficulty. Therefore, the proposed system extracts the characteristic force of each milling layer as the input element for modeling the neural network. This can simplify not only the training model but also achieve the expected bone recognition effect.

The modeling steps are as follows.

**STEP 1 (Preprocessing the Force Signal):** After the system collects all the force signals in the vertebral lamina milling process, it performs a wavelet transformation on the signals to reduce the noise, extracts the force signals in the  $x$ -direction during the single-layer feeding process, and quickly sorts the data. Then, 20% of the data at beginning and end are filtered out to remove force signal fluctuations caused by interference outside the system during milling, such as the drill bit touching the spinous process, sensor acquiring maximum or minimum values, and unintended contact by the operator. Finally, the average of the remaining force data is calculated as the characteristic force signal for the layer (Fig. 8).

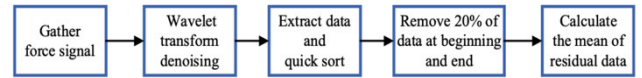


**FIGURE 8.** Processing of milling force data.

**STEP 2 (Normalization of Input Data):** The input data for the bone recognition model in this study include the characteristic single-layer force, milling speed, milling depth, and ultrasonic scalpel power. Because the four-dimensional input data are independent, there may be differences in orders of magnitude between them. Therefore, the data in each dimension need to be normalized using two main methods: the maximum and minimum method and the mean-variance method. In this study, we used the former according to (7).

$$x_k = \frac{x_k - x_{min}}{x_{max} - x_k}, \quad k = 0, 1, \dots, n, \quad (7)$$

where  $x_{min}$  and  $x_{max}$  are the minimum and maximum values of the data sequence, respectively.

**STEP 3 (Establish the BP Neural Network Model):** The neural network was divided into three layers: input, hidden, and output. During the experiment, the boundary between the cortical bone and cancellous bone of the vertebral lamina of living animals was often unclear. This occurred because the surface of the outer cortical bone is not flat, the inner side near the spinous process is higher than the outer side, the articular process side is higher near the upper and lower vertebral bodies than in the middle, and the outer cortical bone surface of different vertebral bodies differ greatly with no clear pattern. The purpose of this study was to realize real-time, accurate, and safe vertebral lamina milling, with a focus on determining the endpoint of the milling operation, i.e., when the milling layer is the inner cortical bone. Therefore, we set the neural network model output layer with one output element and the input layer with four output elements. The hidden layer was selected according to (8).

$$h = \sqrt{m + n} + a, \quad (8)$$

where  $h$  is the number of hidden layers,  $m$  is the number of input layers,  $n$  is the number of output layers, and  $a$  is any value between 1 and 10. For minimizing the model size, the hidden layer was set to have three neurons. Finally, the algorithm model of the neural network shown in Fig. 9 was built.

In this model,  $X_1 - X_4$  are the input elements of the neural network, corresponding to the characteristic milling force, milling speed, milling depth, and ultrasonic scalpel power, respectively;  $H_1 - H_3$  are the intermediate values of the hidden layer; and  $Y$  is the output. For model recognition, to judge whether the current milling layer is the inner cortical bone of the vertebral lamina, the output value is set to 0 or 1.  $V_{v1h} - v_{4h}$  are the weights from the input layer to the hidden layer, and  $w_{11} - w_{31}$  are the weights from the hidden layer to the output layer.

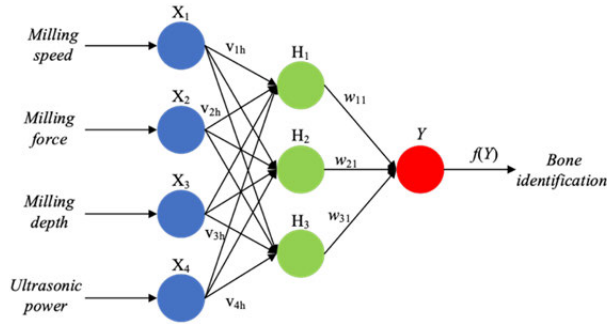


FIGURE 9. BP neural network structure for modeling the milling process.

The forward process of the BP neural network is given by

$$H_j = \sigma\left(\sum_{i=1}^m v_{ij}x_i - a_j\right), \quad (9)$$

$$Y = \sum_{j=1}^h [H_j\omega_j - b], \quad (10)$$

where  $a_j$  is the hidden layer threshold,  $b$  is the output layer threshold, and  $\sigma$  is the neuron activation function. The sigmoid function used in this study is given by

$$\sigma(x) = \frac{1}{1 + e^{-x}}. \quad (11)$$

After the forward process, the error generated by a single process is calculated. Here, the mean square error was selected as the loss function to calculate the error.

$$e = (y - \hat{y})^2 \quad (12)$$

After determining the error, the error value is fed back to the neural network for weight correction during the BP process:

(1) Weight update

$$\begin{aligned} v_{ij} &= v_{ij} + \eta H_j(1 - H_j)x_i\omega_j e \\ \omega_j &= \omega_j + \eta H_j e \end{aligned} \quad (13)$$

(2) Threshold update

$$a_j = a_j + \eta H_j(1 - H_j)\omega_j e \quad b = b + e, \quad (14)$$

where  $\eta$  is the learning rate of the neural network. With repeated iterative calculations of the forward and BP processes,  $v$  and  $w$  are constantly updated until the optimal conditions are met.

In the neural network propagation process, it is necessary to introduce an activation function to adapt the model to nonlinear mapping. When the number of neural network layers is small, a sigmoidal activation function is the optimal choice because it has favorable derivative properties and can map an infinite signal to (0, 1), which is suitable for solving the classification problem in this research [43]. In addition, the convergence error of the neural network was set to  $10^{-4}$ , and the learning rate was set to 0.001.

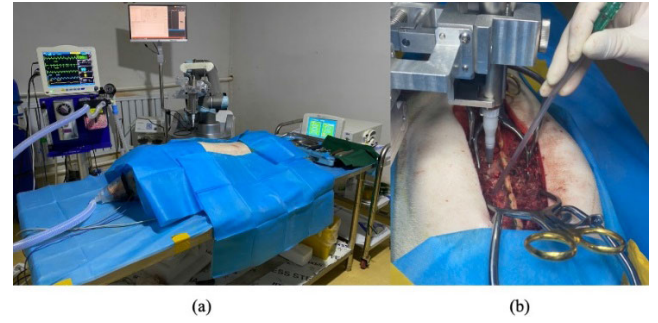


FIGURE 10. Robot-assisted vertebral lamina milling experiment on live pigs: (a) the operating room of animal experiment; (b) the operation process of vertebral lamina milling.

STEP 4 (Set the Threshold Judgment Function of Output Data): When the data in the test set are introduced into the neural network, the output of the output layer is not necessarily an integer of 0 or 1. Therefore, a piecewise function was implemented to set the output intervals of [0, 0.5] and (0.5, 1] to 0 and 1, respectively:

$$f(x) = \begin{cases} 0, & x \in [0, 0.5] \\ 1, & x \in (0.5, 1]. \end{cases} \quad (15)$$

## V. ANIMAL EXPERIMENT VERIFICATION

For verifying the feasibility and accuracy of the proposed model, in this study, we conducted live animal vertebral lamina milling, collected force data, and used the model to test the untrained data. The accuracy rate of bone recognition was used as the evaluation standard. Simultaneously, CT images of the vertebral lamina after milling were acquired to evaluate the milling effect. The same hardware platform as that in the isolated bone experiment was used in the animal experiments. The six-axis force sensor, ultrasonic scalpel holder, and ultrasonic scalpel handle were sequentially fixed to the end of the UR robotic arm, and all components were rigidly connected. During fixing, the feed and vertical directions of the robotic arm were set consistent with the  $x$ - and  $y$ -directions of the force sensor, respectively.

Since the anatomical structure and bone mechanical characteristics of the pig spine are similar to those of the human spine, we selected experimental pigs as the research objects for robot-assisted vertebral lamina milling. This was approved by the ethics committee of the Peking Union Medical Hospital (no. XHDW-2019-027). In this study, a total of six Yorkshire miniature pigs were used, three males and three females, with weights of 35–50 kg and body lengths of 1.2–1.5 m. All pigs were prevented from eating and drinking the day before the operation. Anesthesia was induced by intravenous injection of pentobarbital sodium, isoflurane was administered through inhalation after tracheal intubation to maintain anesthesia, and the vital signs were monitored (Fig. 10).

After anesthesia, the pigs were placed in the prone position. The limbs, chest, back, and buttocks were fixed with bandages to ensure that the position of the spine remained stable



**TABLE 2. Ultrasonic scalpel vertebral lamina milling parameters.**

No.	Milling speed	Scalpel power
1	1 mm/s	60%
2	1 mm/s	80%
3	1 mm/s	100%
4	0.5 mm/s	60%
5	0.5 mm/s	80%
6	0.5 mm/s	100%

\*The milling depth per layer was 0.5 mm in all cases.

and the spinous process was upright. After shaving, disinfection, and draping, the surgeon cut the skin along the median incision on the waist and back. The incision was approximately 15–20 cm in length. The fascia, muscles, and other soft tissues were stripped, bleeding was fully stopped, and the spinal vertebral lamina, spinous process, articular process, and other structures were exposed. The surgeon determined the start and endpoints for vertebral lamina milling and placed the robotic arm end at the starting point, ensuring that it was not in contact with the bone surface. Then, the system was started, and layer-by-layer milling was performed according to the proposed strategy. The milling force signal was transmitted to the PC system on the robotic arm trolley through the acquisition card, data processing and model recognition were performed by the system, and the milling process was terminated by judging the output.

In an actual operation, the surgeon selects different ultrasonic scalpel powers and milling speed according to the specific milling situation. Therefore, to ensure a universal model that can be applied under various robotic surgery conditions, we designed different combinations of milling operation parameters to optimize the model. The most common power of Sonicmed ultrasonic bone scalpel used in spine surgery is 80%, and 60% and 100% power are used in a few cases [44], [45]. There is no standard speed for lamina milling operation. A high milling speed may cause safety problems, whereas a low milling speed will delay the laminectomy [46]. Based on our observation of the actual operation and considering the motion parameters of the UR5 robot, we determined 0.5 mm/s and 1 mm/s as the milling speeds (Table 2). A total of six combinations that satisfy the requirements in both real surgery and engineering experiments were designed. Three sets of experiments were conducted for each combination, yielding a total of 18 datasets. Two datasets were selected for each combination as the training sets and input to the neural network as training parameters. The remaining set was used as the test set to verify the model accuracy. The number in each training set was determined by the number of milling layers, which was between 15 and 18. Because each set of experiments was independent, and the test and training sets were disjointed, the reliability of the final results was guaranteed.

The milling force was normalized before using the training set. The output of the test set before the red line in Fig. 11 was 0, i.e., the milling cutter had not reached the inner cortical

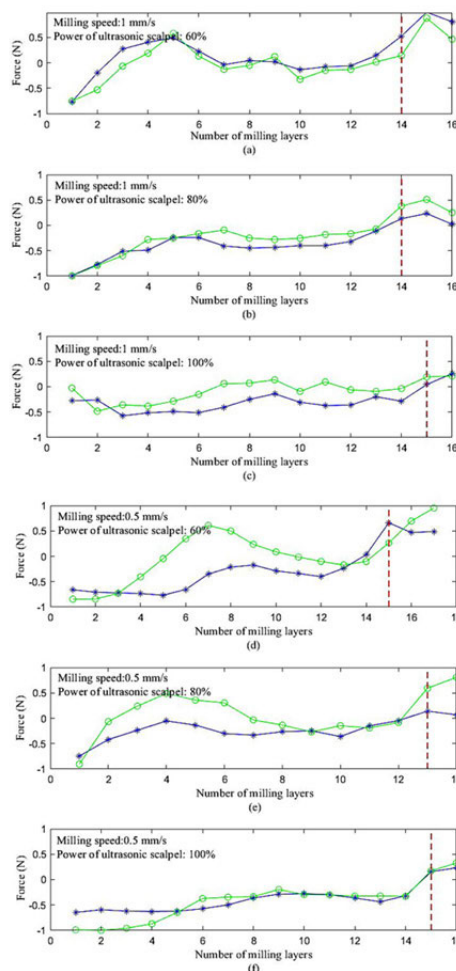


**FIGURE 11. Force characteristics of the neural network input. The green and blue lines represent two parallel experiments, and the red line represents the theoretical junction between the cortical bone and cancellous bone. The ordinate represents the normalized force signal, and the abscissa represents the number of milling bone layers. Experimental conditions: (a) milling speed: 1 mm/s, power of ultrasonic scalpel: 60%; (b) milling speed: 1 mm/s, power of ultrasonic scalpel: 80%; (c) milling speed: 1 mm/s, power of ultrasonic scalpel: 100%; (d) milling speed: 0.5 mm/s, power of ultrasonic scalpel: 60%; (e) milling speed: 0.5 mm/s, power of ultrasonic scalpel: 80%; (f) milling speed: 0.5 mm/s, power of ultrasonic scalpel: 100%.**

bone; the output of the test set after the red line was 1; that is, milling had reached the inner cortical bone. The output was judged based on CT images taken after milling and observation of the cross-section of the vertebral lamina to ensure correct judgment.

From the output corresponding to the test datasets, the distribution of model recognition rates is 85%–100% (Table 3), and the error at the junction between the inner cortical bone and cancellous bone is not more than one layer (Fig. 12). Considering the number of layers in the training set, this error may arise from the difference in bone structure between different vertebral laminae. As the milling depth increases, the difference in the changes in force between layers gradually decreases, which hampers the ability of the model to judge the force characteristics at the junction between the inner cortical bone and cancellous bone.

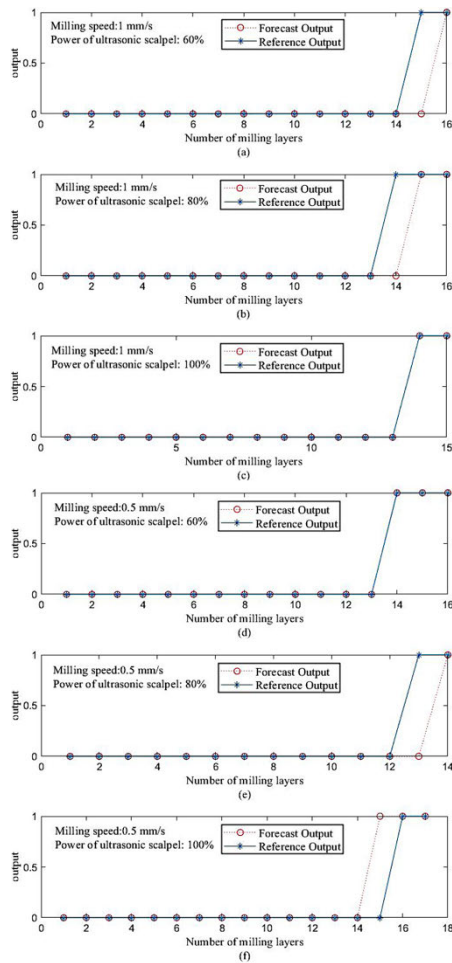


**FIGURE 12.** Output of the neural network, where the red dashed and blue solid lines represent the forecast value from the neural network and reference value, respectively. The ordinate represents the output value of the BP neural network model: 0 indicates that the last layer of cortical bone has not been milled, and 1 indicates that the last layer of cortical bone has been milled. The abscissa represents the milling or grinding depth. Experimental conditions: (a) milling speed: 1 mm/s, power of ultrasonic scalpel: 60%; (b) milling speed: 1 mm/s, power of ultrasonic scalpel: 80%; (c) milling speed: 1 mm/s, power of ultrasonic scalpel: 100%; (d) milling speed: 0.5 mm/s, power of ultrasonic scalpel: 60%; (e) milling speed: 0.5 mm/s, power of ultrasonic scalpel: 80%; (f) milling speed: 0.5 mm/s, power of ultrasonic scalpel: 100%.

**TABLE 3.** Bone recognition rate by neural network.

Working condition group	1	2	3	4	5	6
Recognition rate	100%	93.75%	92.8%	94.4%	94.11%	93.75%

The force signal input of the system is an important indicator of when to stop the milling process. During the milling of each layer, approximately 1200 force signals were collected. Each group contained approximately 14–18 milling layers, and thus the amount of force input data in the training sets was sufficient.

After the experiment, we compared the performance of robot-assisted and manual milling of the vertebral lamina

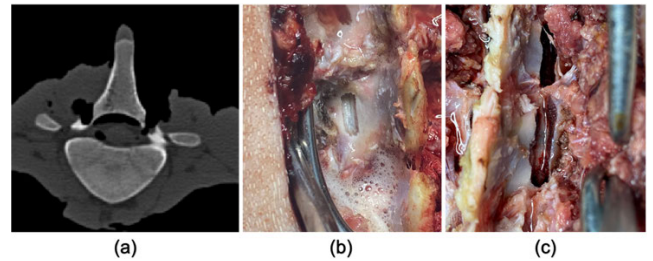


**FIGURE 13.** Animal experiment results: (a) postoperative CT image of the vertebral body, with robot-assisted milling on the left and manual milling on the right; (b) photo of vertebral lamina milled with robotic assistance; (c) photo of manually milled vertebral lamina.

through visual observation and CT imaging (Fig. 13). The bone surface after ultrasonic scalpel milling with robotic assistance was smooth and tidy. The CT image showed that milling occurred in the inner cortical bone. However, the milling depth was not too shallow or deep to cause spinal cord injury. In contrast, the bone surface after manual milling was rough, and the milling path was irregular. The CT image showed that the milling was too deep, the dura mater had been exposed, and there was a risk of spinal cord injury. This comparison shows that the model established in this study can accurately determine the milling ending point and realize safe vertebral lamina milling operation. In addition, the bone recognition rate and milling effect of the model are satisfactory.

**VI. CONCLUSION**

Based on the BP neural network, we developed an algorithmic model suitable for robot-assisted vertebral lamina milling to realize the perception of milling force and recognition of bone layers. This model uses the characteristic milling force, milling speed, milling depth, and ultrasonic scalpel power as input values and outputs whether milling has occurred in the inner cortical bone. The endpoint is judged according to the anatomical structure of the vertebral lamina to achieve safe milling.

The novelty of this study is the application of the bone recognition model and animal experimental verification. First, we used ultrasonic power to establish a bone recognition model based on milling force and optimized the model using data obtained with different milling operation parameters. The achievement not only demonstrates the advanced nature of this work but also meets the current needs of spinal decompression surgery and provides robots with a judgment method that is both versatile and practical. Second, live animal experiments were used for data collection and model verification; this is more in line with the actual situation of decompression surgery. The verification results show that the model has considerable potential for practical applications. In summary, the proposed bone recognition model can significantly improve the safety and reliability of robot-assisted laminectomy and has significant research and translational prospects.

However, there are some limitations in our study. First, although the wavelet transform threshold was used as the optimal filtering and noise reduction method by comparing with Kalman filter and moving average filter, better filtering methods for milling force signals may be available. Second, although the BP neural network used in this study yields a satisfactory recognition rate, the SVMs and fuzzy control are also classical pattern recognition methods that may be more suitable for other milling strategies or different operating environments. The impact of the different filters and pattern recognition methods in improving robot-assisted laminectomy will be investigated in future research.

## REFERENCES

- [1] J. Lurie and C. Tomkins-Lane, "Management of lumbar spinal stenosis," *BMJ*, vol. 352, p. h6234, Jan. 2016.
- [2] O. R. Fjeld, L. Grøvle, J. Helgeland, M. C. Småstuen, T. K. Solberg, J.-A. Zwart, and M. Grotle, "Complications, reoperations, readmissions, and length of hospital stay in 34 639 surgical cases of lumbar disc herniation," *Bone Joint J.*, vol. 101-B, no. 4, pp. 470–477, Apr. 2019.
- [3] J. H. Lee et al., "Nonsurgical treatments for patients with radicular pain from lumbosacral disc herniation," *Spine J.*, vol. 19, pp. 1478–1489, Sep. 2019.
- [4] A. Khosla and A. A. Wagner, "Robotic surgery of the kidney, bladder, and prostate," *Surgical Clin.*, vol. 96, pp. 615–636, Jun. 2016.
- [5] L. Weinberg, S. Rao, and P. F. Escobar, "Robotic surgery in gynecology: An updated systematic review," *Obstetrics Gynecol. Int.*, vol. 2011, Jan. 2011, Art. no. 852061.
- [6] D. Joyce, G. Morris-Stiff, G. A. Falk, K. El-Hayek, S. Chalikhonda, and R. M. Walsh, "Robotic surgery of the pancreas," *World J. Gastroenterol.*, vol. 20, pp. 14726–14732, Oct. 2014.
- [7] M. Shoham, I. H. Lieberman, E. C. Benzel, D. Togawa, E. Zehavi, B. Zilberstein, M. Roffman, A. Bruskin, A. Fridlander, L. Joskowicz, S. Brink-Danan, and N. Knoller, "Robotic assisted spinal surgery—from concept to clinical practice," *Comput. Aided Surg.*, vol. 12, pp. 105–115, Mar. 2007.
- [8] S. Diwan, D. Sayed, T. R. Deer, A. Salomons, and K. Liang, "An algorithmic approach to treating lumbar spinal stenosis: An evidenced-based approach," *Pain Med.*, vol. 20, no. 2, pp. S23–S31, Dec. 2019.
- [9] W.-Y. Lee and C.-L. Shih, "Force control and breakthrough detection of a bone drilling system," in *Proc. IEEE Int. Conf. Robot. Automat. (ICRA)*, Sep. 2003, pp. 1787–1792.
- [10] Y. Sun, L. Wang, Z. Jiang, B. Li, Y. Hu, and W. Tian, "State recognition of decompressive laminectomy with multiple information in robot-assisted surgery," *Artif. Intell. Med.*, vol. 102, Jan. 2020, Art. no. 101763.
- [11] J. J. Craig, *Introduction to Robotics: Mechanics and Control*. Upper Saddle River, NJ, USA: Pearson, 1986.
- [12] N. Hogan, "Impedance control: An approach to manipulation: Part I—Theory," *J. Dyn. Syst., Meas., Control*, vol. 107, no. 1, pp. 1–7, Mar. 1985.
- [13] C. Ott, R. Mukherjee, and Y. Nakamura, "Unified impedance and admittance control," in *Proc. IEEE Int. Conf. Robot. Automat.*, May 2010, pp. 554–561.
- [14] M. W. Spong, S. Hutchinson, and M. Vidyasagar, "Robot modeling and control," *Ind. Robot Int. J.*, vol. 17, no. 5, pp. 709–737, 2006.
- [15] M. Marco, M. Rodríguez-Millán, C. Santiuste, E. Giner, and M. H. Miguélez, "A review on recent advances in numerical modelling of bone cutting," *J. Mech. Behav. Biomed. Mater.*, vol. 44, pp. 179–201, Apr. 2015.
- [16] Y. Hu, H. Jin, L. Zhang, P. Zhang, and J. Zhang, "State recognition of pedicle drilling with force sensing in a robotic spinal surgical system," *IEEE/ASME Trans. Mechatronics*, vol. 19, no. 1, pp. 357–365, Feb. 2014.
- [17] L. Fan, P. Gao, B. Zhao, Y. Sun, X. Xin, Y. Hu, S. Liu, and J. Zhang, "Safety control strategy for vertebral lamina milling task," *CAAI Trans. Intell. Technol.*, vol. 1, no. 3, pp. 249–258, Jul. 2016.
- [18] Y. Kasahara, K. Ohnishi, and H. Kawana, "Analysis of drill wear based on torque and force sensorless cutting power estimation," in *Proc. 36th Annu. Conf. IEEE Ind. Electron. Soc. (IECON)*, Nov. 2010, pp. 1465–1470.
- [19] K. I. A.-L. Al-Abdullah, H. Abdi, C. P. Lim, and W. A. Yassin, "Force and temperature modelling of bone milling using artificial neural networks," *Measurement*, vol. 116, pp. 25–37, Feb. 2018.
- [20] Z. Deng, H. Jin, Y. Hu, Y. He, P. Zhang, W. Tian, and J. Zhang, "Fuzzy force control and state detection in vertebral lamina milling," *Mechatronics*, vol. 35, pp. 1–10, May 2016.
- [21] Y. Sun, H. Jin, Y. Hu, P. Zhang, and J. Zhang, "State recognition of bone drilling with audio signal in robotic orthopedics surgery system," in *Proc. IEEE/RSJ Int. Conf. Intell. Robots Syst.*, Sep. 2014, pp. 3503–3508.
- [22] L. Wen, Z. H. Zhao, J. B. Song, D. D. Yu, M. Chen, and S. G. F. Shen, "Experimental study on thermal and force characteristics in the dry slotting of cortical bone," *Adv. Mater. Res.*, vol. 1136, pp. 233–238, Jan. 2016.
- [23] Y. Dai, Y. Xue, and J. Zhang, "Vibration-based milling condition monitoring in robot-assisted spine surgery," *IEEE/ASME Trans. Mechatronics*, vol. 20, no. 6, pp. 3028–3039, Dec. 2015.
- [24] T. Vercellotti, "Technological characteristics and clinical indications of piezoelectric bone surgery," *Minerva Stomatol.*, vol. 53, no. 5, pp. 207–214, May 2004.
- [25] *Essentials in Piezosurgery: Clinical Advantages in Dentistry*, Vercellotti, Minneapolis, MN, USA, 2016.
- [26] B. J. Schaller, R. Gruber, H. A. Merten, T. Kruschat, H. Schliephake, M. Buchfelder, and H. C. Ludwig, "Piezoelectric bone surgery: A revolutionary technique for minimally invasive surgery in cranial base and spinal surgery? Technical note," *Operative Neurosurg.*, vol. 57, p. E410, Oct. 2005.
- [27] S. Schaeren, C. Jaquier, M. Heberer, M. Tolnay, T. Vercellotti, and I. Martin, "Assessment of nerve damage using a novel ultrasonic device for bone cutting," *J. Oral Maxillofacial Surg.*, vol. 66, pp. 593–596, Mar. 2008.
- [28] Y. Otake, M. Nakamura, A. Henmi, T. Takahashi, and Y. Sasano, "Experimental comparison of the performance of cutting bone and soft tissue between piezosurgery and conventional rotary instruments," *Sci. Rep.*, vol. 8, no. 1, pp. 1–7, Dec. 2018.
- [29] J. Esteves, E. Marcantonio, Jr., A. de Souza Faloni, F. R. Rocha, R. Marcantonio, K. Wilk, and G. Intini, "Dynamics of bone healing after osteotomy with piezosurgery or conventional drilling—Histomorphometrical, immunohistochemical, and molecular analysis," *J. Transl. Med.*, vol. 11, no. 1, p. 221, 2013.
- [30] X. Banse, T. J. Sims, and A. J. Bailey, "Mechanical properties of adult vertebral cancellous bone: Correlation with collagen intermolecular cross-links," *J. Bone Mineral Res.*, vol. 17, no. 9, pp. 1621–1628, Sep. 2002.
- [31] D. T. Reilly and A. H. Burstein, "The mechanical properties of cortical bone," *J. Bone Joint Surg.*, vol. 56, no. 5, pp. 1001–1022, 1976.
- [32] G. J. Tortora and N. P. Anagnostakos, *Principles of Anatomy and Physiology*. New York, NY, USA: HarperCollins, 1996.
- [33] G. Van Ham, K. Denis, J. V. Sloten, R. Van Audekerke, G. Van der Perre, J. De Schutter, E. Aertbeliën, S. Demey, and J. Bellemans, "Machining and accuracy studies for a tibial knee implant using a force-controlled robot," *Comput. Aided Surg.*, vol. 3, no. 3, pp. 123–133, Jan. 1998.
- [34] *Ultrasonic Surgical System*. Accessed: Jan. 6, 2021. [Online]. Available: <https://www.sonicmed.com.cn>
- [35] F. W. Lewis, S. Jagannathan, and A. Yesildirek, *Neural Network Control of Robot Manipulators and Non-Linear Systems*. Boca Raton, FL, USA: CRC Press, 1999.
- [36] H. K. Khalil and J. W. Grizzle, *Nonlinear Systems*. Upper Saddle River, NJ, USA: Prentice-Hall, 2002.
- [37] P. A. Ioannou and J. Sun, *Robust Adaptive Control*. North Chelmsford, MA, USA: Courier Corporation, 2012.
- [38] *Universal Robot*. Accessed: Dec. 5, 2020. [Online]. Available: <https://www.universal-robots.cn>
- [39] J. Chen, Z. Li, J. Pan, G. Chen, Y. Zi, J. Yuan, B. Chen, and Z. He, "Wavelet transform based on inner product in fault diagnosis of rotating machinery: A review," *Mech. Syst. Signal Process.*, vols. 70–71, pp. 1–35, Mar. 2016.
- [40] D. L. Donoho and I. M. Johnstone, "Ideal spatial adaptation by wavelet shrinkage," *Biometrika*, vol. 81, no. 3, pp. 425–455, Sep. 1994.
- [41] D. Valencia, D. Orejuela, J. Salazar, and J. Valencia, "Comparison analysis between rigrsure, sqtwolog, heursure and minimaxi techniques using hard and soft thresholding methods," in *Proc. 21st Symp. Signal Process., Images Artif. Vis. (STSIVA)*, Aug. 2016, pp. 1–5.
- [42] I. Daubechies, "Orthonormal bases of compactly supported wavelets," *Commun. Pure Appl. Math.*, vol. 41, no. 7, pp. 909–996, Oct. 1988.
- [43] F. Guan, Y. Sun, X. Qi, Y. Hu, G. Yu, and J. Zhang, "State recognition of bone drilling based on acoustic emission in pedicle screw operation," *Sensors*, vol. 18, no. 5, p. 1484, May 2018.

- [44] X. Hu, D. D. Ohnmeiss, and I. H. Lieberman, "Use of an ultrasonic osteotome device in spine surgery: Experience from the first 128 patients," *Eur. Spine J.*, vol. 22, no. 12, pp. 2845–2849, Dec. 2013.
- [45] X. Lu, Y. Zhao, X. Zhao, D. Qi, X. Yang, X. Wang, R. Zhou, Y. Jin, and B. Zhao, "Efficacy and safety analysis of ultrasonic bone curette in the treatment of thoracic spinal stenosis," *Orthopaedic Surg.*, vol. 11, no. 6, pp. 1180–1186, Dec. 2019.
- [46] H.-T. Chen, C.-C. Hsu, M.-L. Lu, S.-H. Chen, J.-M. Chen, and R.-W. Wu, "Effects of combined use of ultrasonic bone scalpel and hemostatic matrix on perioperative blood loss and surgical duration in degenerative thoracolumbar spine surgery," *BioMed Res. Int.*, vol. 2019, May 2019, Art. no. 6286258.



**HAO QU** was born in Changchun, Jilin, China, in 1993. He received the M.M. degree from Jilin University, Jilin, in 2018. He is currently pursuing the M.D. degree in orthopedics with Peking Union Medical College Hospital, Beijing, China.

His research interests include orthopedics, spinal surgery robot, and human factors.



**BAODUO GENG** was born in Beijing, China, in 1996. He received the B.S. degree from North China Electric Power University, Beijing, in 2019. He is currently pursuing the M.S. degree in mechanical engineering and automation with Beihang University, Beijing.

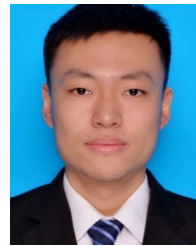


**BINGRONG CHEN** was born in Yulin, Guangxi, China, in 1996. He received the B.S. degree from Peking University, Beijing, China, in 2021. He is currently pursuing the M.M. degree in orthopedics with the Peking Union Medical College Hospital, Beijing.



**JIAN ZHANG** was born in Shanxi, China, in 1993. He received the M.S. degree from Beihang University, Beijing, China, in 2018, where he is currently pursuing the D.S. degree in mechanical engineering and automation.

His main research interests include medical robotics and automation control.



**YONGLIANG YANG** (Member, IEEE) received the B.S. degree in electrical engineering from Hebei University, Baoding, China, in 2011, and the Ph.D. degree in electrical engineering from the University of Science and Technology Beijing (USTB), Beijing, China, in 2017. From 2015 to 2017, he was a Visiting Scholar with the Missouri University of Science and Technology, Rolla, MO, USA, sponsored by the China Scholarship Council. He is currently an Associate Professor with the

School of Automation and Electrical Engineering, USTB. His research interests include adaptive optimal control, distributed optimization and control, and cyber-physical systems.



**LEI HU** received the B.S. and M.S. degrees in mechanical engineering and automation from Beihang University, Beijing, in 1986 and 2007, respectively, and the Ph.D. degree from Harbin Engineering University, Harbin, in 2015.

He is currently a Professor with the School of Mechanical Engineering and Automation, Beihang University. His research interests include medical robot, mechanical design, and mechatronics.



**YU ZHAO** received the B.S. degree in pediatrics and the M.M. degree in orthopedics from China Medical University, Shenyang, China, in 1993 and 1999, respectively, and the M.D. degree from the Peking Union Medical College Hospital, Chinese Academy of Medical Sciences and Peking Union Medical College, Beijing, China, in 2002.

He is currently a Professor with the Department of Orthopedics, Peking Union Medical College Hospital. He has published several articles in well-known international academic journals in the spine field cited by SCI. His research interests include thoracic spinal stenosis, spinal deformity, bioabsorbable orthopedics materials, and robot-assisted spinal surgery.

...